Contrasting Eastern-Pacific and Central-Pacific Types of ENSO

Hsun-Ying Kao and Jin-Yi Yu[1]

Department of Earth System Science
University of California, Irvine
Irvine, CA 92697-3100

October 29, 2007

Submitted to *Journal of Climate*

1. *Corresponding author address*: Dr. Jin-Yi Yu, Department of Earth System Science, University of California, Irvine, CA 92697-3100. E-mail: jyyu@uci.edu

ABSTRACT

In this study, surface observation and subsurface ocean assimilation datasets are examined to contrast two distinct types of El Niño Southern Oscillation (ENSO): an eastern-Pacific (EP) type and a central-Pacific (CP) type. An analysis method combining Empirical Orthogonal Function analysis and linear regression is used to separate these two ENSO types. The EP-type of ENSO is found to have its sea surface temperature (SST) anomaly center located in the eastern equatorial Pacific and attached to the coast of South America. This type of ENSO is associated with basin-wide thermocline and surface wind variations and shows a strong teleconnection with the tropical Indian Ocean. In contrast, the CP-type of ENSO has most of its surface wind, SST, and subsurface anomalies confined in the central Pacific and tends to onset, develop, and decay in-situ. This type of ENSO does not involve thermocline variation and is likely forced by the atmosphere. It has a stronger teleconnection with the Southwestern Indian Ocean. Phase-reversal signatures can be identified in the anomaly evolutions of the EP-ENSO but not for the CP-ENSO. This implies that the CP-ENSO may occur more as events or epochs than as a cycle. The EP-ENSO has experienced a stronger interdecadal change with the dominant period of its SST anomalies shifted from 2 years to 4 years near 1976/77, while the dominant period for the CP-ENSO stayed near the 2-year band. ENSO indices based on ocean heat content (OHC) were developed to identify these two types of ENSO during the period of 1958-2001. It is found that the OHC indices can better capture and separate these two types of ENSO than SST-based ENSO indices. During the analysis period, most of the strong El Niño events tend to be EP-type of ENSO while most of the strong La Niña events tend to be CP-type of ENSO, indicating a spatial asymmetry between strong El Niño and La Niña events. It is also noticed that a strong

CP-type of La Niña tends to follow a strong EP-type of El Niño. Weaker ENSO events could be combinations of both types of ENSO.

1. Introduction

El Niño Southern Oscillation (ENSO) is characterized by sea surface temperature (SST) variations in the eastern and central equatorial Pacific. The canonical ENSO event portrayed by Rasmusson and Carpenter (1982) typically develops from the South America Coast and propagates westward along the equatorial Pacific. It has been noticed that ENSO SST anomalies could also start from the central equatorial Pacific and spread toward the eastern Pacific (e.g., Wang 1995). Efforts were made to examine different types of ENSO in the tropical Pacific. ENSO events were usually classified according to their periodicity, interval, onset time, or the associated zonal SST structure (e.g., Yasunari 1985; Fu et al. 1986; Barnett 1991; Enfield and Cid 1991, Xu and Chan 2001). Various numbers of ENSO types were identified in those studies. However, it appears that the shift of SST anomaly center between the eastern and central equatorial Pacific is a common contrasting feature between/among these various types of ENSO. For example, Fu et al. (1986) noticed that El Niño SST anomalies show two major patterns: one with an anomalous warming center in the eastern Pacific and the other in the central Pacific. In another example, Xu and Chan (2001) categorized El Niño events according to their onset time and concluded that there are two types of El Niño events: one onsets in spring and the other in summer. Although not emphasized by the authors, it is noticed from their results that the composite SST anomalies for the spring-onset type concentrate in the eastern equatorial Pacific but concentrate in the central Pacific for the summer-onset type. Trenberth and Stepaniak (2001) were among the first to recognize that different characters and evolutions of ENSO events could not be fully accounted for without considering the SST contrast between the eastern and central equatorial Pacific. They used two ENSO SST indices to characterize ENSO evolutions: a Niño3.4 (5°S-5°N,

170°W-120°W) SST index to represent the averaged SST anomalies in the eastern-to-central Pacific and a Trans-Niño Index (TNI) to represent the gradient of ENSO SST anomalies between the eastern and central Pacific. They defined TNI as the difference between the normalized Niño1+2 (10°S-0°, 80°-90°W) and Niño4 (5°S-5°N, 160°E-150°W) SST indices. By analyzing the lead-lag correlation between Niño3.4 and TNI, they recognized the ENSO evolutions in the past hundred years, including a shift in 1976/77. A very recent study by Ashok et al. (2007) further argued that there exists a type of ENSO that is different from the canonical ENSO whose spatial pattern is characterized by out-of-phase SST anomalies between the central Pacific and the eastern and western Pacific along the equator. All these studies indicate that zonal shift of SST anomaly patterns between the eastern and central equatorial Pacific is one of the most obvious features to separate different types of ENSO.

Yu and Kao (2007) noticed that all the four Niño SST indices in the eastern-to-central Pacific, i.e., the Niño1+2, Niño3 (5°S-5°N, 150°W-90°W), Niño3.4, and Niño4 indices, have very different decadal changes in their persistence barriers. In their study, the happening season of the persistence barrier is identified as the season of the year that the lagged auto-correlation of its SST anomalies drops to a small value most quickly than rest of the year, meaning SST anomalies are least persistent in that particular season of the year. They found that the persistence barriers for central-Pacific SST indices (i.e., the Niño3.4 and Niño4 indices) stayed in the boreal spring in the past four decades (1958-2001) while the persistence barriers for eastern-Pacific SST indices (i.e., the Niño1+2 and Niño3 indices) changed from decade to decade. The different decadal changes in the timing of the persistence barriers imply that ENSO SST evolutions in the central and

eastern equatorial Pacific are probably controlled by different physical mechanisms. By analyzing subsurface ocean information, Yu and Kao (2007) further found the decadal change in the persistence barriers of eastern-Pacific SST indices coincided with the decadal change of mean ocean heat content (OHC) along the equatorial Pacific. They suggested that there may be two types of ENSO: an eastern-Pacific (EP) type that locates in the eastern Pacific and whose generation mechanism involves thermocline variations along the entire equatorial Pacific, and a central-Pacific (CP) type that locates in the central tropical Pacific and whose generation is not related to the thermocline variations. Observed ENSO events do exhibit distinct SST patterns that laid support to the existence of the EP and CP types of ENSO. Two examples are shown in Figure 1: the 1997/98 and 1977/78 El Niño events. For the 1997/98 El Niño (Figure 1a), its SST anomalies are mostly located in the eastern part of the tropical Pacific, extending from the South America Coast around 80ºW to 160ºW and covering the Niño1+2 and Niño3 regions (see Figure 1c). For the 1977/78 El Niño (Figure 1b), its SST anomalies during the peak phase of the event are mostly concentrated in the central equatorial Pacific from 160ºE to 120ºW, covering the Niño3.4 and Niño4 regions (see Figure 1d).

In this study, we aim to examine these two different types of ENSO by contrasting their surface and subsurface structures and evolutions, associated atmosphere-ocean coupling, and teleconnection. An analysis method that combines linear regression and Empirical Orthogonal Function (EOF) is used to separate these two types of ENSO from SST observations. Currently, SST indices have been used extensively to identify ENSO indices because of their availability. Subsurface ocean temperature information has become more available from XBT or satellite observations and assimilations and has

provided critical information about ENSO dynamics. Recent studies have increasingly use OHC information to describe and predict ENSO. In this study, we develop two OHC indices to explore the possibility of better identifying and separating the EP- and CP-types of ENSO. This paper is organized as following: The datasets used in this study are described in Section 2. The characteristics of the EP- and CP-ENSO and their teleconnection patterns are contrasted in Section 3. OHC-based ENSO indices for these two types of ENSO are presented in Section 4 and are used to identify ENSO events during 1958-2001 in Section 5. The results are summarized and discussed in Section 6.

2. Datasets

Four datasets were used in this study. For SST, we used the 1°x1° Met Office Hadley Center's Sea Ice and Sea Surface Temperature dataset (HadISST) (Rayner et al., 2003). The SST data is available from 1870 until present. Here, we only used the more reliable data after 1950 for analyses. For subsurface ocean temperature information, we used the assimilation product from Simple Ocean Data Assimilation (SODA; Carton et al. 2000a, b) for the period of 1958-2001. The SODA dataset has 40 levels unevenly divided from 5m to 5374m and covers the global oceans from 75.25°S to 89.25°N with a horizontal resolution of 0.5°x0.5°. The thermocline depth is identified in this study by vertical interpolation of ocean temperature profile. Surface wind stresses information was obtained from NOAA's National Center for Environmental Prediction/National Centre for Atmospheric Research NCEP/NCAR Reanalysis (Kalnay et al. 1996). Monthly means from this reanalysis have a horizontal resolution of 2.5°x2.5° and are available from 1948-2007. The precipitation data used in this study is from Global Precipitation

Climatology Project (GPCP) (Adler et al., 2003), which is available from 1979 to 2007 and has a horizontal resolution of 2.5°x2.5°. In this paper, anomalies of all variables are defined as the deviations from their long-term mean in the corresponding month.

3. Spatial and Temporal Characteristics of the EP- and CP-Types of ENSO

We used the EOF analysis method to extract the spatial patterns of the EP- and CP-types of ENSO (hereafter EP- and CP-ENSO) from the HadISST dataset. Our EOF analysis procedure is different from those used in Trenberth and Stepaniak (2001) and Ashok et al. (2007). In order to separate the influence of these two types of ENSO in the tropical Pacific region (30ºS-30ºN, 120ºE-80ºW), we removed their correlation parts from the SST anomalies before the EOF analysis was applied. To obtain the CP-ENSO structure with the EOF analysis, we first subtracted the anomalies regressed with the Niño1+2 index from the original SST anomalies. Similarly, we subtracted the SST anomalies regressed with the Niño4 index from the original SST anomalies before the EOF analysis was applied to identify the leading structure of the EP-ENSO. Figure 2 shows the two leading EOF modes obtained from the aforementioned procedures. The leading EOF mode shown in Figure 2a represents the EP-type of ENSO, which explains 36% of the residual SST variance after the Niño4-regression part of the anomalies is removed. This EP-type of ENSO is characterized by SST anomalies extending from the South America Coast into the central Pacific along the equator. The SST anomalies are mostly contained in the Niño1+2 and Niño3 regions. This structure is similar to the leading EOF structure obtained from the original SST anomalies (i.e., without removing the regression part, not shown here), but less extending into the central Pacific. Figure 2b

shows the structure of the CP-type of ENSO, which has SST anomalies mostly confined in the central Pacific between 160ºE and 120ºW, covering the Niño3.4 and Niño4 regions. This EOF mode explains 38% of the residual SST variance. It is interesting to notice that this EOF mode has its SST anomalies extending from the central Pacific toward the northeastern subtropical ocean outside Mexico and Central America. The peak SST anomaly pattern shown in Figure 1b for the 1977/78 El Niño event is very similar to this CP-ENSO pattern.

The principal components (PC) of these two leading EOFs are shown in Figure 3a and Figure 4a. It is noticed that both time series are not symmetric with respect to the zero value. They tend to skew toward either the positive or negative values. The skewness coefficients for the PCs of the EP- and CP-type of EOFs are 1.18 and -0.45, respectively. A larger value of positive (negative) skewness denotes more extreme warm (cold) events. The skewness indicates that the EP-type of ENSO tends to appear more often as strong El Niño events than as strong La Niña events. On the other hand, the CP-type of ENSO tends to appear more often as strong La Niña events than as strong El Niño events. Our results are consistent with the recent observational study of Sun and Yu (2007), in which they showed that strong El Niño events tend to locate in the eastern Pacific and attach to the South America Coast, while strong La Niña events tend to detach from the coast and center in the central Pacific. Jin et al. (2007; personal communication) also reported that the El Niño events with SST anomalies centered in the cold tongue region tend to be stronger than the El Niño events with SST anomalies centered in the warm pool region.

Also shown in Figures 3 and 4 are the wavelet power spectra of these two PCs. The dash lines in Figures 3b and 4b denote the 95% significant level and the values below the curves are uncertain. Figure 3b shows that the EP-type of ENSO has two dominate periods: one near the 2-year band and the other near the 4-year band. The EP-ENSO tends to occur every 2 years before the 1976/77-climate shift but every 4 years after the shift. This is consistent with the previous report that ENSO periodicity shifted from two years to about four years around 1976/77 (An and Wang, 2000). The skewness coefficient of the principal component of this leading EOF increases from 0.31 for the period of 1950-1976 to 1.43 for the period of 1977-2006, reflecting the fact that more intense El Niño's appear in the eastern Pacific after 1976/77, such as 1982/83 and 1997/98 El Niño's. Figure 4b shows that the principal component of the leading EOF for the CP-ENSO has a significant power near the 1-2year bands, which does not shift abruptly around 1976/77. These results suggest that the EP-type of ENSO has experienced a stronger decadal/interdecadal change with its properties shifted near 1976/77, while the decadal change is relatively small for the CP-type of ENSO.

In addition to the differences in their spatial structure, the EP- and CP-types of ENSOs also show differences in their temporal evolutions. Figure 5 shows the lagged correlation coefficients between the PCs of the two leading EOFs and SST anomalies in the tropical Pacific. The 95% confidence level is 0.29 with a two-tailed student-t test. With a 0.3 contour interval, most of the contours shown here are significant. For the EP-type of ENSO (Figure 5a), the SST anomalies emerge from the coast of South America, propagate westward to the central Pacific, and decay off equator. The peak SST anomalies of this type of ENSO appear near the coasts, accompanying with weaker and

opposite anomalies in the equatorial western Pacific. For the CP-type of ENSO (Figure 5b), SST anomalies first appear around the dateline, develop and mature in a v-shape anomaly structure extending toward the subtropics in both hemispheres (but more into the northern hemisphere), and then decay in the equatorial central Pacific. The CP-ENSO has larger associations with SST anomalies in the subtropics than the EP-ENSO. In addition, the propagating feature of the SST anomalies in the CP-type of ENSO is weaker and less clear than those of the EP-type of ENSO.

We noticed that these two types of ENSO have even larger differences in their subsurface temperature evolutions. Figure 6 shows the vertical cross-sections of the lagged correlation coefficients between the PCs of the leading EOFs and the subsurface ocean temperature averaged between 5ºS and 5ºN in the Pacific. For the EP-type of ENSO (Figure 6a), large and out-of-phase temperature anomalies in the subsurface ocean appear on both sides of the Pacific basin. Temperature anomalies in the eastern tropical Pacific originate from the American coasts and then propagate westward on the surface (see the panels from Lag –6 months to Lag 2 months). At the same time, negative subsurface anomalies were accumulated in the western Pacific. After the mature phase of the event, these subsurface temperature anomalies propagate eastward along the thermocline and eventually emerge on the surface of the eastern Pacific and reverse the phase of ENSO. This evolution is similar to those described by the delayed oscillator theory of ENSO (Battisti and Hirst 1989; Suarez and Schopf 1988). In contrast, the subsurface temperature evolution of the CP-ENSO (Figure 6b) does not have a basin-wide fluctuation pattern and shows little propagation feature. The initiation, development, and termination of the subsurface temperature anomalies all occur in the central Pacific.

The anomalies appear first near the surface and then extend downward to a shallow layer of about 100 meters. This depth is well above the local thermocline, which is about 150-200 meters deep, indicating that thermocline variation is not involved in the evolution of the CP-type of ENSO. It is important to note that there is no identifiable phase-reversal signal in Figure 6b, implying that the CP-type of ENSO may be not a self-sustained cycle/oscillation like the EP-ENSO. The CP-ENSO probably occurs as an event that is not driven by thermocline variations, while the EP-ENSO is driven by delayed-oscillator type of thermocline variations and occurs as cycle with its warm and phase events following each other. Discussions of whether ENSO should be viewed as event or cycle (e.g., Kessler 2002) might be aided by recognizing that there are two types of ENSO that behave as event in one type and as cycle in the other.

4. Indices for EP- and CP-types of ENSO

An important feature in Figure 6 is that the subsurface temperature anomalies associated with the EP- and CP-types of ENSO are almost orthogonal to each other in space. The subsurface temperature variation associated with the EP-ENSO has a nodal point located in the central Pacific where the CP-type of ENSO produces the largest subsurface anomalies. This property suggests that ENSO indices based on subsurface ocean information may be more capable of separating these two types of ENSO than ENSO indices based on SST anomalies. As mentioned earlier, the subsurface temperature variation of the CP-ENSO is mostly confined in the upper one hundred meters in the central Pacific Ocean, which is shallower than the thermocline depth in this region. Therefore, the traditional definition of OHC that averages ocean temperatures in the

upper 300 meters is not suitable for capturing the subsurface temperature variation related to the CP-ENSO. Here, we explore the possibility of constructing ENSO indices based on the upper 100 meters of OHC information to better examine and separate the EP- and CP-types of ENSO. Based on the largest subsurface temperature anomalies found in Figure 6, we choose to average the upper-100m ocean temperature anomalies in the two box regions indicated in Figure 7 as the OHC indices for the EP- and CP-types of ENSO (hereafter EP OHC and CP OHC indices). This depth is deep enough to include the thermocline in the eastern equatorial Pacific, whose variation is important to the evolution of the EP-type of ENSO. As shown in Figure 7, the long-term mean thermocline depth (represented by the 20° isotherm) is less than 100m in this region. Since ocean temperature anomalies associated with ENSO events are larger in the eastern Pacific than in the central Pacific, the averaged temperature anomalies are normalized before being used to construct the OHC indices.

Figure 8 and 9 show the time series and power spectrum for the EP OHC and CP OHC indices. A 5-month running mean was applied to smooth both time series. The skewness coefficients of the time series (1958-2001) are 1.68 for the EP OHC index and –0.63 for the CP OHC index. These values are larger than those calculated from the principal components of the leading EOFs (cf. Figures 3 and 4). The skewness coefficients indicate that the preference of the EP-type for El Niño and the CP-type fro La Niña is more obvious in the OHC-based indices than in the SST-based indices. Most strong El Niño events defined by the Niño3.4 SST index were identifiable in the EP OHC index of Figure 8a, including the 1972/73, 1976/77, 1982/83, 1991/92, and 1997/98 events. In contrast, most large La Niña events defined by the Niño3.4 SST index were

identifiable only by the CP OHC index shown in Figure 9a, including the 1973/74, 1975/76, 1983/84, 1988/89, and 1998/99 events. It should be noted that the different dominant periods between the EP- and CP-types of ENSO become more obvious with the OHC indices. Figures 8b and 9b show that the EP index has a 99% significant power peak near the 3~4-year band, and the CP index has a significant power peak near the 2-year band. It should be noted that the correlation coefficient between the EP and CP OHC indices is 0.27, which is smaller than the correlation coefficient between the two PC indices (which is –0.48). Therefore, our analyses suggest that ENSO indices based on subsurface ocean temperature anomalies appear more capable of separating the EP- and CP-types of ENSO than SST-based ENSO indices.

We repeat the analyses of Figures 5 and 6 with the two OHC indices to further examine the structures and evolutions of the EP- and CP-types of ENSO. For the CP-ENSO, the results are similar to those obtained with the PCs of the leading EOFs (not shown here). But for the EP-ENSO, the OHC index reveals some different evolutions. Figure 10 shows the lagged correlation coefficients of the EP OHC index with the SST and subsurface temperature anomalies in the tropical Pacific. For SST (Figure 10a), the anomalies start from the coastal region and propagate westward to the central Pacific, which is similar to those shown in Figure 5. Whereas, the maximum SST extending more to the central Pacific, and the SST anomalies dissipate off equator after the events (see panels from Lag 4 months to Lag 10 months). This pattern shows the discharge phase of the recharge-discharge theory (Jin 1997). For subsurface temperature anomalies (Figure 10b), the OHC anomalies start from the western-to-central Pacific and then propagate eastward and upward along the thermocline until they reach the eastern Pacific, where

they combine with the OHC anomalies from the coastal region. The temperature anomalies then emerge to the surface and further spread westward as the event grows. At the same time, opposite subsurface temperature anomalies begin to form in the western-to-central Pacific at a depth of about 100m. These opposite OHC anomalies later propagate along the thermocline and eventually reverse the phase of ENSO in the eastern Pacific. The OHC index links the life cycle of the EP-ENSO to ocean wave propagations more clearly than the SST-based indices do.

We further examine the atmosphere-ocean coupling and teleconnection features of these two types of ENSO by correlating their OHC indices with atmospheric anomalies in the Indo-Pacific region. Figure 11 shows the correlation coefficients with surface wind anomalies. We highlight the coefficients that pass the 95% significance level estimated by a two-tailed t-test. The figure shows that the EP-type of ENSO is associated with significant wind stress anomalies covering a large part of the tropical Pacific. On the other hand, surface wind anomalies associated with the CP-type of ENSO are limited to the equatorial western Pacific (130ºE-160ºW) and off Australia. The differences in the wind stress patterns further support our suggestion that the EP-ENSO is related to basin-wide coupling processes, while the CP-ENSO is related to local coupling processes in the central Pacific. Figure 12 shows the lagged correlation coefficients with precipitation anomalies. For EP-ENSO (Figure 12a), the precipitation anomalies extend from the equatorial eastern to central Pacific, where the largest SST anomalies locate. There are opposite precipitation anomalies near Indonesia and Amazon regions. The precipitation anomaly pattern associated with this type of ENSO reflects zonal shifts of the Pacific Walker Circulation. An EP-type of El Niño event shifts the rising branch of

the circulation from far western Pacific to the center-to-eastern Pacific, and vice versa for a La Niña event of the same type. For CP-ENSO (Figure 12b), the precipitation anomalies are characterized by a dipole pattern within the tropical Pacific, with largest anomalies located mainly in the far western and eastern Pacific. It is noticed that the positive and negative anomaly centers of this dipole pattern does not line up in the same latitude. Instead, they tend to locate slightly to the north and to the south of the equator respectively. The anomaly pattern appears related to the meridional shift of the intertropical convergence zone (ITCZ). During the warm phase of CP-ENSO, the ITCZ intensifies in the equatorial western Pacific and shift more northward in the eastern Pacific, and vice versa for the cold phase of the CP-ENSO. The impacts of CP-ENSO events on precipitation are much less in Indonesia and negligible in Amazon.

Figure 12 also indicates that the EP-ENSO can influence the precipitation anomaly in the Indian Ocean, which appears as a weak zonal anomaly dipole along the equator. No such influence is observed for the CP-ENSO in the Indian Ocean. The dipole-type of precipitation anomalies is accompanied with a SST anomaly dipole in the equatorial Indian Ocean, which could be seen in the lagged correlation coefficients shown in Figure 13a between the EP OHC index and the Indo-Pacific SST. In addition to the EP-ENSO SST patterns already described in Figure 10a, this figure further shows that the EP-type of ENSO is associated with an Indian Ocean Dipole (IOD) SST pattern (Saji et al., 1999; Webster et al., 1999) that tends to occur during/after the peak ENSO phase. Surface wind stress anomalies associated with the EP-ENSO also appear along equatorial Indian Ocean (See Figure 11a), which is known to coexist with the IOD (Saji et al. 1999; Webster et al. 1999). After the EP-ENSO reaches its peak phase, the western anomaly

center of the IOD spreads toward the east and evolves into a basin-wide warming or cooling. This IOD and Indian Ocean warming sequence is similar to that discussed by An (2004) and Yu and Lau (2004). Results presented here suggest that there are certain correlations between EP-ENSO and IOD. Figure 13b shows that the CP-type of ENSO has a weaker correlation with the Indian Ocean SST variations, locating in the Southern Indian Ocean near 20ºS. This pattern of SST anomalies is similar to the regression of SST and ENSO index in February and March studied by Xie et al. (2001). The surface wind anomalies for the CP-ENSO shown in our Figure 11b are similar to the wind stress anomalies they obtained for the southern Indian Ocean SST variability. Figure 13 implies that the EP-type of ENSO is more effective in establishing the teleconnection between the ENSO and the tropical Indian Ocean, while the CP-type of ENSO influencing the Southwestern Indian Ocean SST more.

5. Case Identifications for 1958-2001

In this section, we use the OHC indices to identify EP- and CP-types of ENSO events for the period of 1958-2001. Figure 14 shows the scattering of the monthly values of EP and CP OHC index from 1958 to 2001. The size of every dot is proportional to the value of Niño3.4 SST index in the corresponding month, indicating the strength of ENSO. We use this figure to examine how different strengths of ENSO (measured by Niño3.4 SST index) are projected onto as the EP- or CP-types of ENSO. The dots are colored red for strong El Niño events (with the Niño3.4 SST index larger than 1ºC) and blue for large La Niña events (with the Niño3.4 SST index smaller than 1ºC). It is easy to notice from the figure that almost all the large La Niña events (the blue dots) are

projected onto the coordinate of CP OHC index; with the OHC index value changes approximately proportioned to the Niño3.4 index value (i.e., the dot size). For these events, the EP OHC index values are in general fixed at a small value (about -0.7). These features conform again that strong La Niña events tend to appear as CP-type of La Niña. Although a little less obvious, a similar tendency can be found for large El Niño events (the large red dots). A large portion of the red dots is projected onto the coordinate of EP OHC index with their CP OHC index values fixed more-or-less at a small value (about 1.0). This tendency again shows that most strong El Niño events tend to appear as EP-type of El Niño. Sun and Yu (2007) argue that the spatial asymmetry between El Niño and La Niña, like the one shown here, provides a way for the ENSO cycle (including the El Niño and La Niña phases) to leave a non-zero impact on the Pacific basic state. They postulated that this ENSO-basic state interaction mechanism slowly modifies the basic SST state and the ENSO intensity, and as a result, give rise to a decadal modulation of ENSO intensity.

We then identify El Niño and La Niña events from the time series of the EP and CP OHC indices. When the EP/CP index of an event is larger or smaller than one standard deviation (1.3ºC for EP and 0.55ºC for CP) for more than 5 consecutive months, the event is identified as an EP- or CP-ENSO event. The identified event is categorized as a weak event if the absolute index value is smaller than two standard deviations, and as a strong event if the value is larger than two standard deviations. Table 1 summarizes all the strong and weak EP- and CP-ENSO events based on these criteria during the period of 1958-2001. The table shows that the EP type contains all the strong El Niño events, and no extreme cold event occurs as the EP type. On the opposite, the CP type contains

every extreme cold event but no intense warm events. However, weak El Niño tends to appear as CP-type in many cases. In some particular years, both the EP- and CP-types of ENSO occurred. For example in 1982/83, a strong EP-type El Niño and a weak CP-type of El Niño occurred simultaneously in the tropical Pacific.

Based on events identified in Table 1, we constructed composite lifecycle for the strong EP- and CP-ENSO. The month of peak ENSO intensity of every event is used as the center month of the composite. During the composite analyses, we noticed that a strong CP-type La Niña often follows a strong EP-type El Niño. This tendency can be identified from Table 1. For instance, the strong CP-type La Niña's of 1973/74, 1983/84, and 1998/99 came after the strong EP-type El Niño's of 1972/73, 1982/83, and 1997/98. The composite lifecycle is shown in Figure 15. For strong EP-type of El Niño (Figure 15a), SST anomalies concentrate in the eastern Pacific, which is similar to the canonical El Niño defined by Rasmusson et al. (1982). After the warm event (about 6 to 18 months after the peak), it comes negative SST anomalies, which originate from the central Pacific and develop into a CP-type of La Niña. For strong CP-type of La Niña (Figure 15b), the negative SST anomalies start from the central Pacific between 180º and 120ºW. The event develops and decays in the central Pacific without an evident propagation. About a year before the La Niña, there is an EP-type of El Niño. The composite shown in Figure 15 further confirms the tendency for strong EP-type El Niño and CP-type La Niña to occur subsequently and alternatively. The right panels in Figure 15 display the normalized values of the EP, CP and Niño3.4 indices during the events. They show that the EP OHC index captures the evolution of warm events better while the CP OHC index captures the evolution of cold events better. Niño3.4 index generally has a value between

EP and CP indices. Consistent with the suggestion of Trenberth and Stepaniak (2001), the Niño3.4 SST index is able to represent the general temperature variations in the equatorial Pacific, but is not as good as the EP/CP OHC index in separating the EP- and CP-types of ENSO.

6. Conclusions and Discussion

Two different types of ENSO are described and contrasted in this paper according to their spatial structure. Based on the centers of their SST anomalies, we term these two ENSO types the eastern-Pacific ENSO and central-Pacific ENSO. The EP-ENSO is closer to the canonical ENSO and fits very well with the evolution described by the delayed-oscillator theory of ENSO. This type of ENSO appears to be a basin-wide coupling phenomenon, which relies on thermocline variations for its generation and phase reversal. The CP-type of ENSO has most of its associated SST, surface wind, and subsurface ocean variations confined in the central equatorial Pacific. This type appears to arise from local atmosphere-ocean coupling in the region, which involves only a shallow layer (about 100 meters) of subsurface ocean temperature variations. Since this ENSO type starts its development from surface, it is likely that local atmospheric forcing is important to this type of ENSO, such as those associated with Madden and Julian oscillation (Madden and Julian 1971) and Asian or Australian monsoons. It is noticed that the CP-ENSO does not have a phase-reversal feature in its evolution, while such a feature can be identified for the EP-ENSO. Our results suggest that the EP-ENSO may arise from basin-wide subsurface ocean memory mechanism and appears as a cycle/oscillation, while the CP-ENSO may be a local coupling event (rather than a cycle) that requires

atmospheric forcing to trigger its occurrence. These two ENSO types also exhibit different teleconnection with the Indian Ocean, with the EP-ENSO links more closely with the tropical Indian Ocean while the CP-ENSO links more with the Southern Indian Ocean.

The results presented in this paper suggest that there is a need to define and separate ENSO indices to better monitor the different types of ENSO activity. We have explored in this study the possibility of developing new OHC indices to better separate the EP- and CP-types of ENSO. We found that the EP/CP indices calculated from OHC information can measure all the warm or cold SST anomalies occur in the equatorial Pacific, including some events that Niño3.4 fails to capture. For example, in May 1966 (not shown here), the warm SST shows up in the equatorial Pacific, but was not captured by the Niño3.4 index. However, EP index captures the heat content variations near the coastal region during this event. Also in January 1991, the Niño3.4 index again failed to capture the warming in the central Pacific, west to the Niño3.4 region, but CP index is able to reveal this central Pacific event. With more and more ocean assimilation datasets available nowadays, such as German Estimating the Circulation and Climate of the Ocean (GECCO) generated by University of Hamburg and data assimilation produced by Bureau of Meteorology Research Center (BMRC), we should be able to take advantages of the improved subsurface ocean information to better understand the ENSO evolutions and apply the OHC information for better ENSO predictions.

Acknowledgments. The authors benefited from the discussions with Dr. Tony Lee of JPL. The research was support by NASA (NNX06AF49H), NSF (ATM-0638432), and

JPL (subcontract No.1290687). Data analyses were performed at University of California, Irvine's Earth System Modeling Facility and the San Diego Supercomputer Center. The SODA data is downloaded from http://iridl.ledo.columbia.edu/SOURCES/.CARTON-GIESE/SODA, the HadISST data is downloaded from http://hadobs.metoffice.com/hadisst/data/download.html, and the Niño3.4 SST anomalies is downloaded from http://www.cpc.noaa.gov/products/analysis_monitoring/ensostuff/ensoyears.shtml.

References

Adler, R.F., G.J. Huffman, A. Chang, R. Ferraro, P. Xie, J. Janowiak, B. Rudolf, U. Schneider, S. Curtis, D. Bolvin, A. Gruber, J. Susskind, P. Arkin, and E. Nelkin, 2003: The Version 2 Global Precipitation Climatology Project (GPCP) Monthly Precipitation Analysis (1979-Present). *J. Hydrometeor.*, **4**,1147-1167.

An, S.-I., and B. Wang, 2000: Interdecadal change of the structure of ENSO mode and its impact on the ENSO frequency. *J. Climate*, **13**, 2044-2055.

An, S-I, 2004: A dynamical linkage between the monopole and dipole modes in the tropical Indian Ocean. *Theor Appl Climatol*, **78**, 195–201.

Ashok K., S. Behera, A. S. Rao, H. Weng, T. Yamagata, 2007: El Niño Modoki and its teleconnection. *J. Geophys Res*. (*accepted*)

Barnett, T. P., M. Latif, E. Kirk, and E. Roeckner, 1991: On ENSO physics. *J. Climate*, **4**, 487-515.

Battisti, D. S. and A. C. Hirst, 1989: Interannual variability in the tropical atmosphere-ocean system: Influence of the basic state, ocean geometry, and nonlinearity. *J. Atmos. Sci.*, **46**, 1687-1712.

Carton, J. A., G. A. Chepurin, X. Cao, and B. S. Giese, 2000a: A simple ocean data assimilation analysis of the global upper ocean 1950-1995, Part I: Methodology, *J. Phys.*

Oceanogr., **30**, 294-309.

Carton, J. A., G. A. Chepurin, X. Cao, 2000b: A simple ocean data assimilation analysis of the global upper ocean 1950-1995, Part II: Reseults. *J. Phys. Oceanogr.*, **30,** 311-326.

Enfield, D.B., and L. Cid S., 1991: Low-frequency changes in El Niño-Southern Oscillation. *J. Climate*, **4**, 1137–1146.

Fu, C., H. F. Diaz, and J. O. Fletcher, 1986: Characteristics of the response of sea surface temperature in the central Pacific associated with warm episodes of the Southern Oscillation. *Mon. Wea. Rev*., **114**, 1716-1738.

Jin, F.F., 1997: An equatorial ocean recharge paradigm for ENSO. Part I: Conceptual Model. *J. Atmos. Sci*., **54**, 811-829.

Kalnay, E., M. Kanamitsu, R. Kistler, W. Collins, D. Deaven, L. Gandin, M. Iredell, S. Saha, G. White, J. Woollen, Y. Zhu, M. Chelliah, W. Ebisuzaki, W. Higgins, J. Janowiak, K.C. Mo, C. Ropelewski, J. Wang, and A. Leetmaa, 1996: The NCEP/NCAR 40-year reanalysis project. Bull. *Amer. Meteor. Soc*., **77**, 437-471.

Kessler, W. S., 2002: Is ENSO a cycle or a series of events? *Geophys. Res. Lett.*, **29**(23), 2125.

Madden, R. A., and P. R. Julian, 1971: Detection of a 40-50 day oscillation in the zonal wind in the tropical Pacific. *J. Atmos. Sci*., **28**, 702-708.

Rasmusson, E. M. and T. H. Carpenter, 1982: Variations in tropical sea-surface temperature and surface wind fields associated with the Southern Oscillation El-Niño. *Mon. Wea. Rev.*, **110**, 354-384.

Rayner, N.A., D.E. Parker, E.B. Horton, C. K. Folland, L. V. Alexander, D. P. Rowell, E.C. Kent, and A. Kaplan, 2003: Global analyses of sea surface temperature, sea ice, and night marine air temperature since the late nineteenth century. *J. Geophys. Res*., **108**, 4407.

Saji, N. H., B. N. Goswami, P. N. Vinayachandran and T. Yamagata, 1999: A dipole mode in the tropical Indian Ocean. *Nature*, **401**, 360-363.

Suarez, M. J. and P. S. Schopf, P. S., 1988: A delayed action oscillator for ENSO. *J. Atmos. Sci*., **45**, 3283-3287.

Sun, F. and J.-Y. Yu, 2007: A 10-15 year modulation cycle of ENSO intensity*, submitted to J. Climate.*

Trenberth, K. E., D. P. Stepaniak, 2001: Indices of El Niño evolution. *J. Climate*, **14**, 1697-1701.

Wang, B., 1995: Interdecadal changes in El Niño onset in the last four decades. *J. Climate*, **8**, 167-285.

Webster, P. J., A. M. Moore, J. P. Loschnigg, and R. R. Leben, 1999: Coupled ocean-atmosphere dynamics in the Indian Ocean during 1997-98. *Nature*, **401**, 356-360.

Xie, S.-P., H. Annamalai, F. Schott, and J. P. McCreary Jr., 2001: Structure and mechanisms of South Indian Ocean climate variability. *J. Climate*, **15**, 864-874.

Xu J. J. and J. C. L. Chan, 2001: The role of the Asian-Australian monsoon system in the onset time of El Niño events. *J. Climate*, **14**, 418-433.

Yasunari, T., 1985: Zonally propagating modes of the global east-west circulation associated with the Southern Oscillation. *J. Meteor. Soc. Japan*, **63**, 1013-1029.

Yu, J.-Y. and K. M. Lau, 2004: Contrasting Indian Ocean SST variability with and without ENSO influence: A coupled atmosphere-ocean GCM study. *Meteorology and Atmospheric Physics*, DOI: 10.1007/s00703-004-0094-7.

Yu, J.-Y., H.-K. Kao, 2007: Decadal changes of ENSO persistence barrier in SST and ocean heat content indices 1958-2001. *J. Geophys. Res.*, **112**.

List of Figure Captions

Figure 1. Examples of the eastern-Pacific and central-Pacific types of ENSO: (a) SST anomalies averaged from November 1997 to January 1998 of the 1997/98 El Niño event and (b) SST anomalies averaged from November 1977 to January 1978 of the 1977/78 El Niño event. The Niño regions covered by each type of ENSO are illustrated in (c) for the eastern-Pacific type and in (d) for the central-Pacific type. Red contours in (c) and (d) outline the region of SST anomaly patterns of these two ENSO types. Contour intervals are 0.5°C for (a) and 0.3°C for (b).

Figure 2. Leading EOF patterns obtained from a combined EOF-regression analysis for (a) the eastern-Pacific type of ENSO and (b) the central-Pacific type of ENSO. Contour intervals are 0.1. The numbers indicated in the upper-left corners are the percentage of variance explained by each EOF.

Figure 3. The (a) time series and (b) wavelet power spectrum of the principal component of the eastern-Pacific type of ENSO. Dash lines denote the 95% significant level and the values below the curves are uncertain.

Figure 4. Same as Figure 3 but for the principal component of the central-Pacific type of ENSO.

Figure 5. Lagged correlation coefficients between the principal components of (a) EP and

(b) CP EOF with SST anomalies in the tropical Pacific. Contour intervals are 0.3. The 95% confidence level is 0.29 with a two-tailed student-t test.

Figure 6. Lagged correlation coefficients between the principal components of the (a) EP and (b) CP EOF and ocean temperature anomalies averaged between 5ºS and 5ºN. Contour intervals are 0.3.

Figure 7. Vertical cross-section of the mean ocean temperatures along the equatorial Pacific (5ºS-5ºN). The two boxes indicate the regions used to define the OHC indices for the EP-ENSO (80ºW-90ºW) and CP-ENSO (160ºE-150ºW). Both boxes cover from the ocean surface to 100m deep. Contour intervals are 2ºC. The thick-dashed line is the 20ºC isotherm and is used to indicate the thermocline depth.

Figure 8. (a) Time series and (b) power spectrum of the normalized EP OHC index. The red curve represents the 99% significance level.

Figure 9. Same as Figure 8 but for the CP OHC index.

Figure 10. Lagged correlation coefficients between the EP OHC index and (a) SST anomalies and (b) subsurface ocean temperature anomalies in the tropical Pacific. Contour intervals are 0.3.

Figure 11. Lagged correlation coefficients between surface wind anomalies and the OHC index of the (a) EP-ENSO and (b) CP-ENSO. Correlation vectors that pass the 95% confidence levels are highlighted.

Figure 12. Lagged correlation coefficients between precipitation anomalies and the OHC index of the (a) EP-ENSO and (b) CP-ENSO. Contour intervals are 0.3 ºC.

Figure 13. Lagged correlation coefficients between SST anomalies and the OHC index of (a) EP-ENSO and (b) CP-ENSO. Contour intervals are 0.3 ºC.

Figure 14. Scattering plot of standardized monthly values of the EP and CP OHC indices from 1958 to 2001. The dot size is proportional to the value of Niño3.4 SST index in the corresponding month. The coordinate is the value of EP OHC index. The abscissa is the value of the CP OHC index.

Figure 15. Composite lifecycle of SST anomalies along the eqiatorial Pacific for (a) strong EP-type of El Niño events and (b) strong CP-type of La Niña events. The center month of the composite is the month of peak value of the OHC index. Contour intervals are 0.4°C. The right panels show the corresponding EP OHC index (blue dot-dashed), CP OHC index (red dashed), and Niño3.4 SST index (black).

Table 1. Classification of strong and weak El Niño and La Niña events based on the time series of the EP and CP OHC Indices during 1958-2001. Events are classified as weak events if its index value is between one and two standard deviation and as strong event if its value is larger than two standard deviations. See the text for a more detailed explanation of the classification.

	EP	**CP**
Strong El Niño	72-73, 82-83 91-92, 97-98	None
Weak El Niño	76-77	63-64, 77-78,79-80 82-83, 86-87, 90-91 91-92, 94-95
Strong La Niña	None	73-74, 75-76, 83-84 88-89, 98-99
Weak La Niña	84-85	64-65, 70-71, 99-00

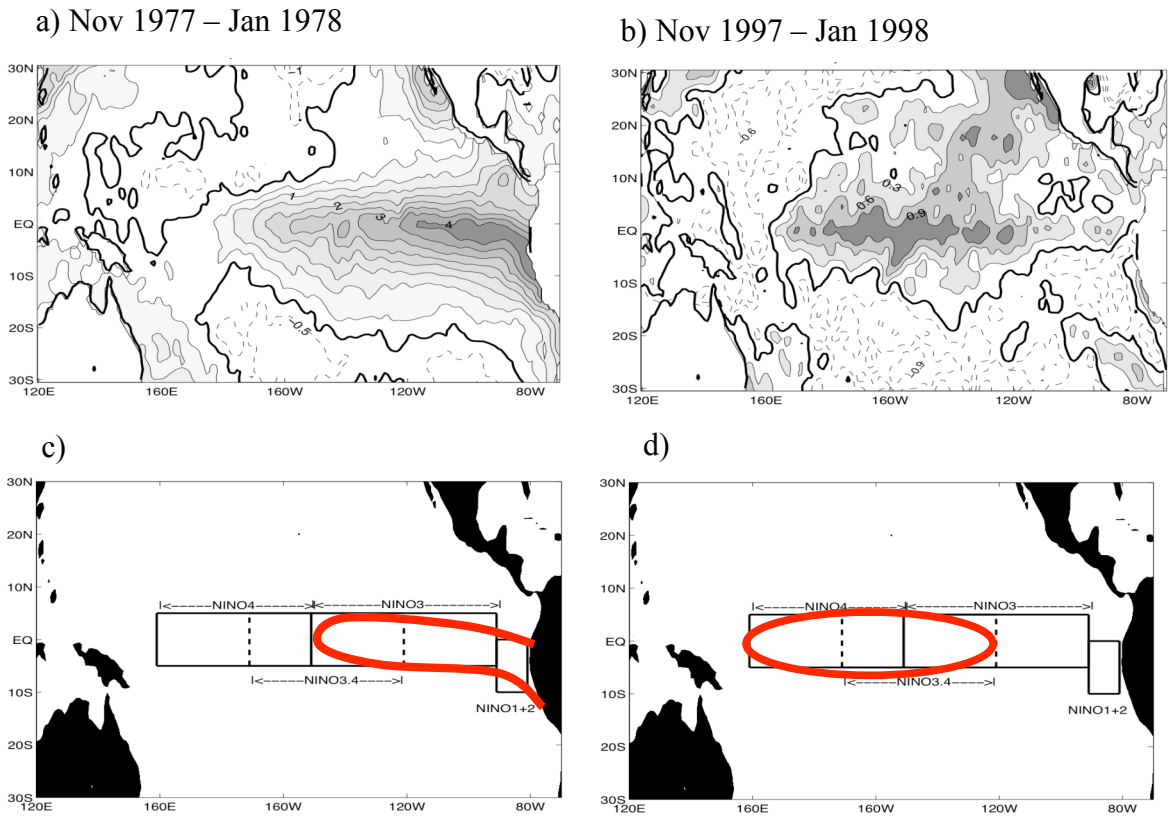


Figure 1. Examples of the eastern-Pacific and central-Pacific types of ENSO: (a) SST anomalies averaged from November 1997 to January 1998 of the 1997/98 El Niño event and (b) SST anomalies averaged from November 1977 to January 1978 of the 1977/78 El Niño event. The Niño regions covered by each type of ENSO are illustrated in (c) for the eastern-Pacific type and in (d) for the central-Pacific type. Red contours in (c) and (d) outline the region of SST anomaly patterns of these two ENSO types. Contour intervals are 0.5°C for (a) and 0.3°C for (b).

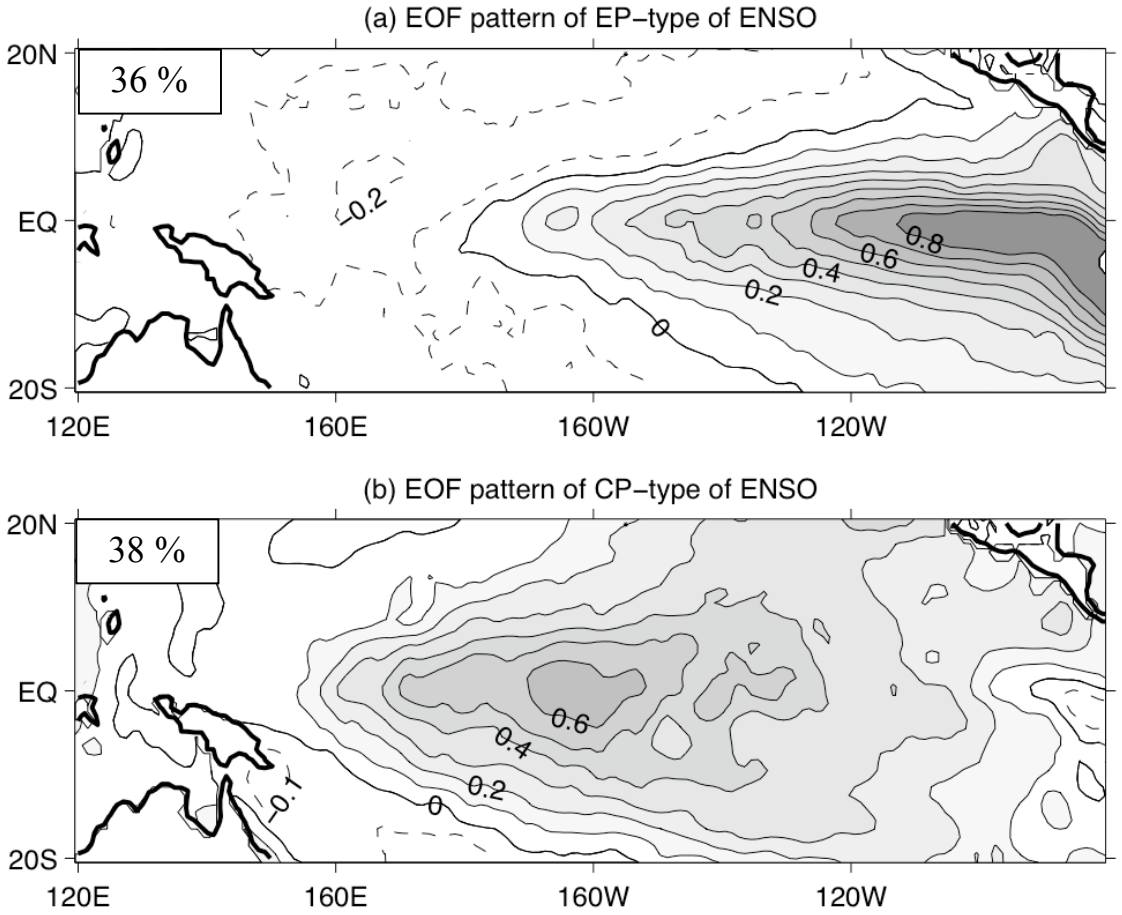


Figure 2. Leading EOF patterns obtained from a combined EOF-regression analysis for (a) the eastern-Pacific type of ENSO and (b) the central-Pacific type of ENSO. Contour intervals are 0.1. The numbers indicated in the upper-left corners are the percentage of variance explained by each EOF.

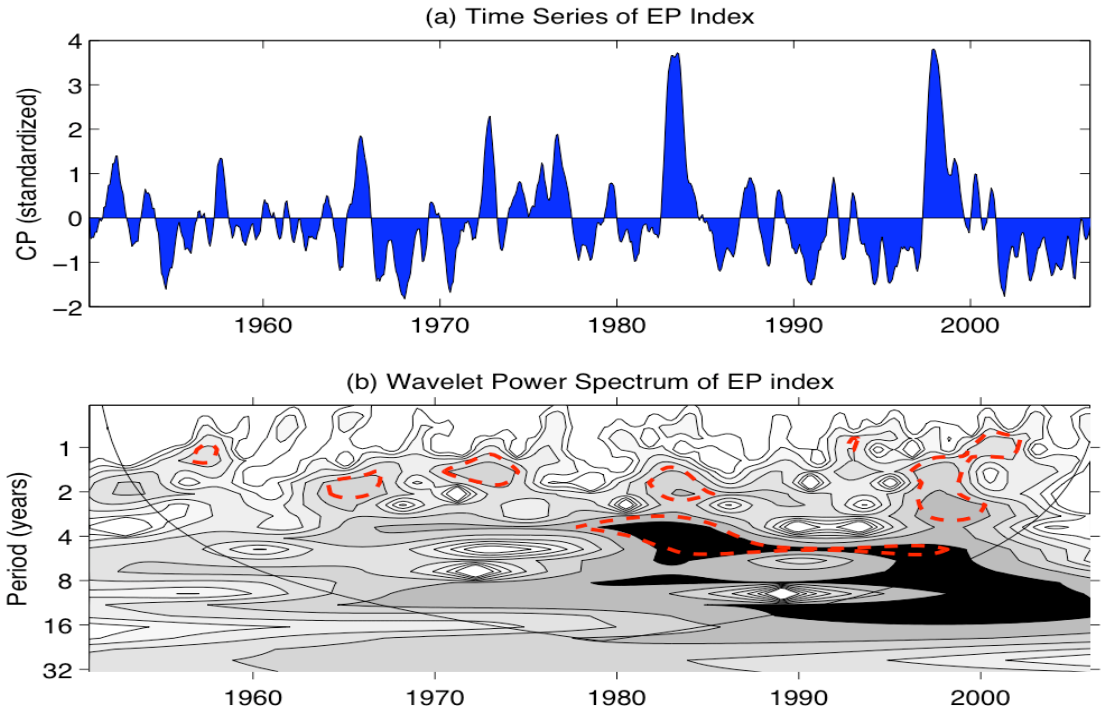


Figure 3. The (a) time series and (b) wavelet power spectrum of the principal component of the eastern-Pacific type of ENSO. Dash lines denote the 95% significant level and the values below the curves are uncertain.

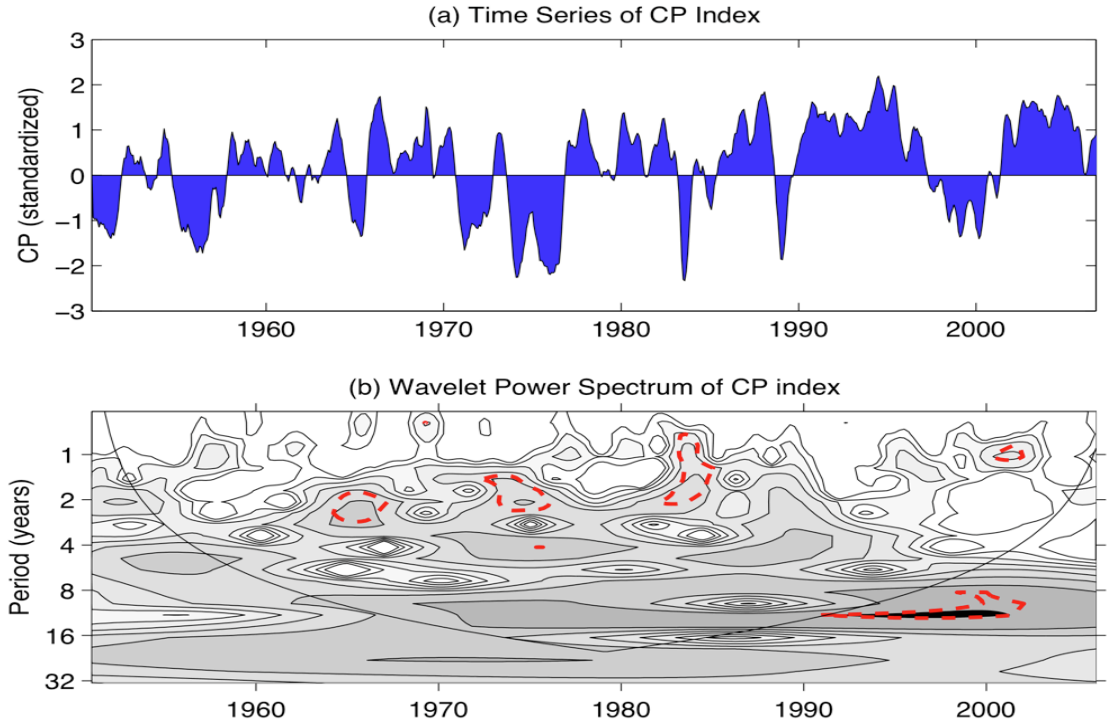
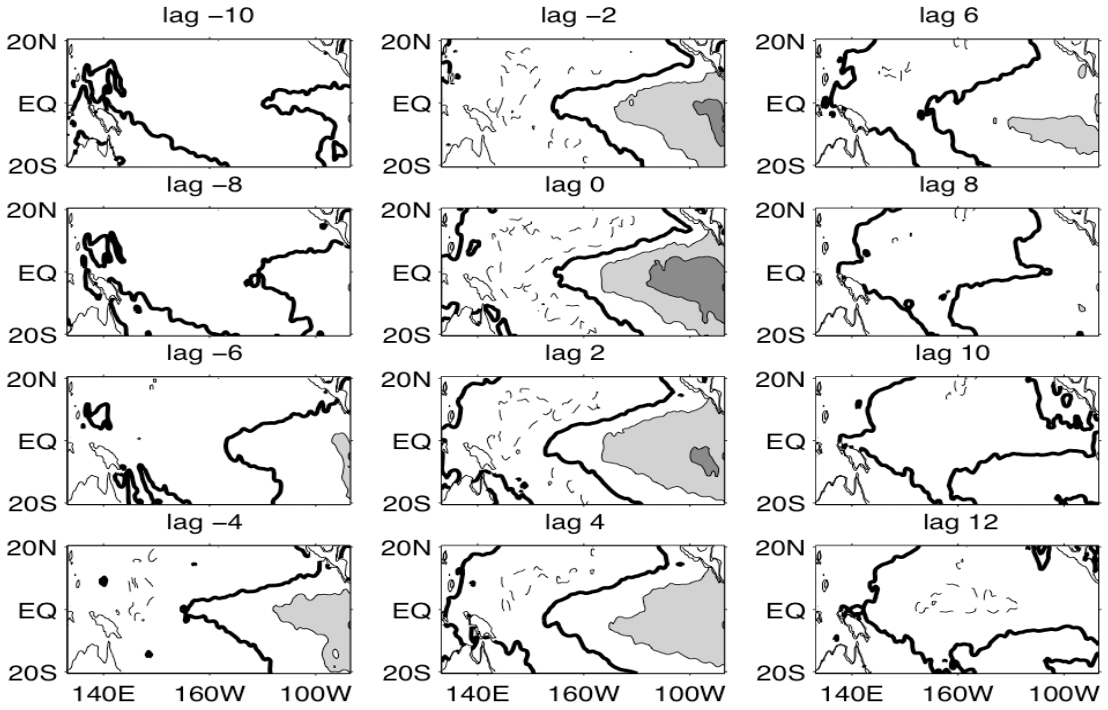


Figure 4. Same as Figure 3 but for the principal component of the central-Pacific type of ENSO.

(a) Lagged-correlation of PC1 of EP and SST



(b) Lagged-correlation of PC1 of CP and SST

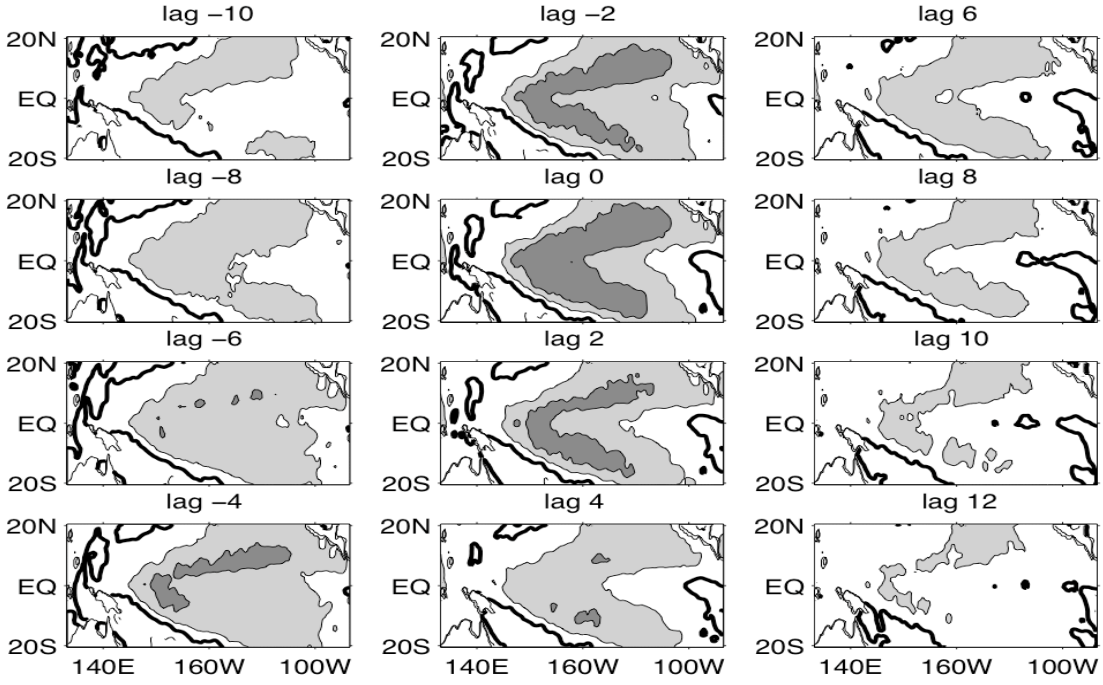
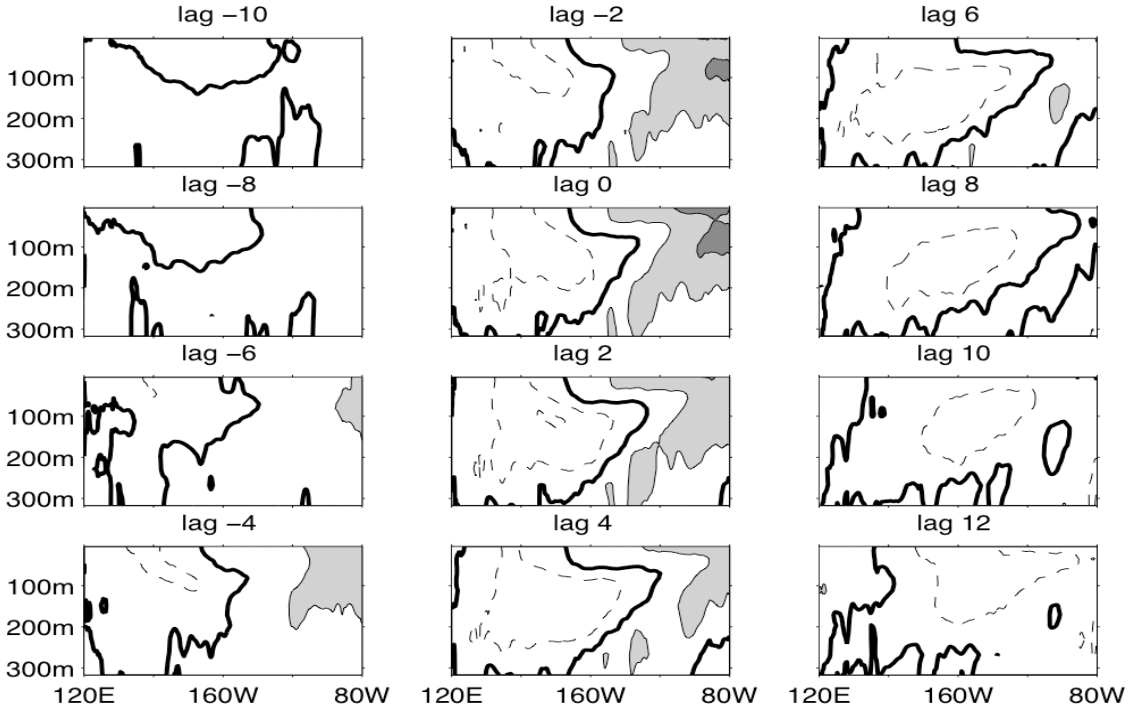


Figure 5. Lagged correlation coefficients between the principal components of (a) EP and (b) CP EOF with SST anomalies in the tropical Pacific. Contour intervals are 0.3. The 95% confidence level is 0.29 with a two-tailed student-t test.

(a) Lagged-correlation of PC1 of EP and ocean temperature



(b) Lagged-correlation of PC1 of CP and ocean temperature

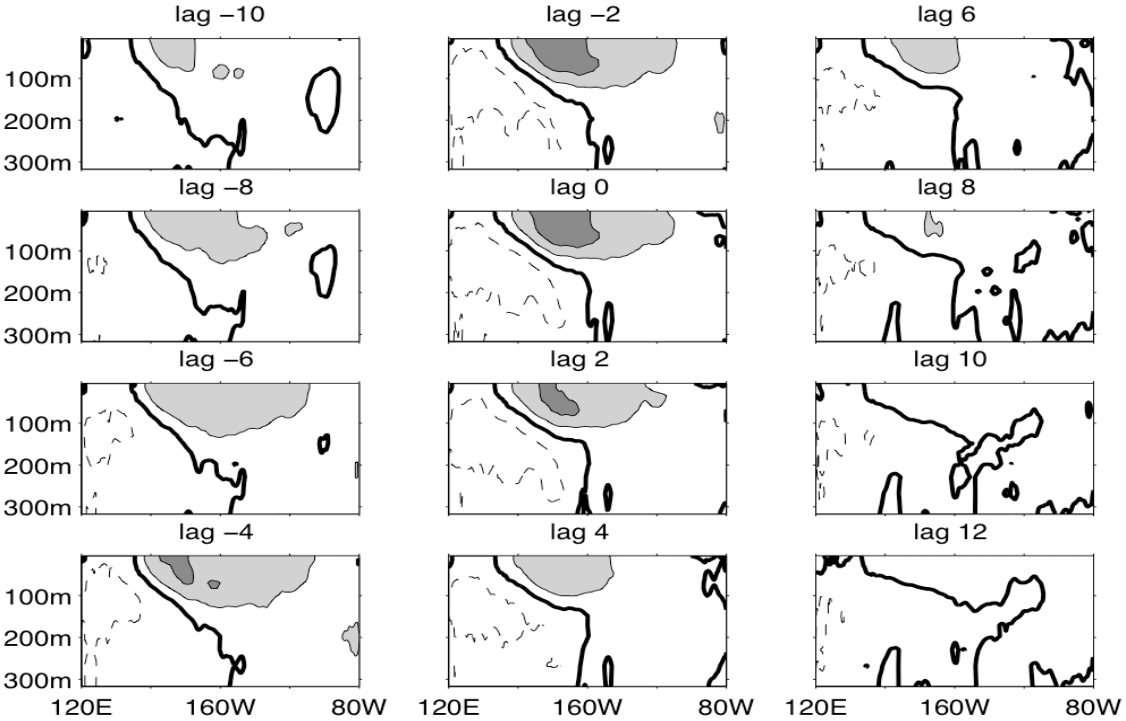


Figure 6. Lagged correlation coefficients between the principal components of the (a) EP and (b) CP EOF and ocean temperature anomalies averaged between 5ºS and 5ºN. Contour intervals are 0.3.

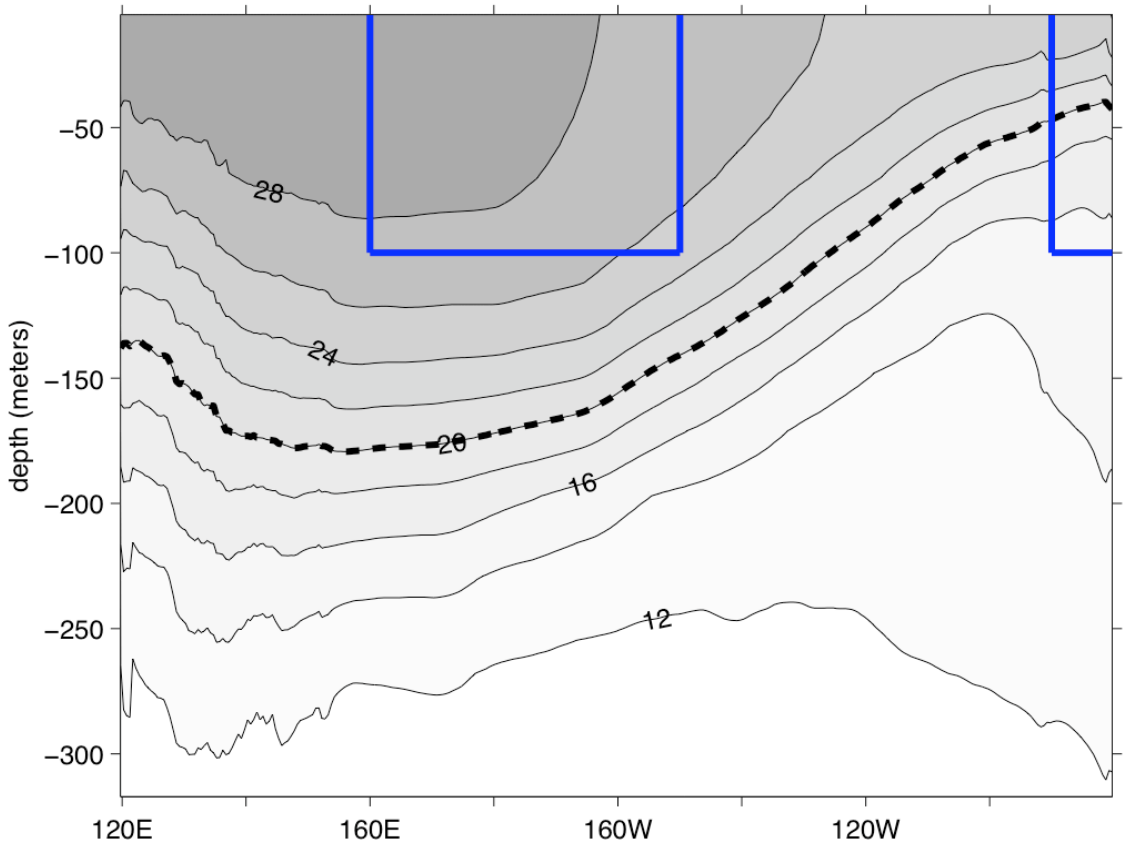


Figure 7. Vertical cross-section of the mean ocean temperatures along the equatorial Pacific (5ºS-5ºN). The two boxes indicate the regions used to define the OHC indices for the EP-ENSO (80ºW-90ºW) and CP-ENSO (160ºE-150ºW). Both boxes cover from the ocean surface to 100m deep. Contour intervals are 2ºC. The thick-dashed line is the 20ºC isotherm and is used to indicate the thermocline depth.

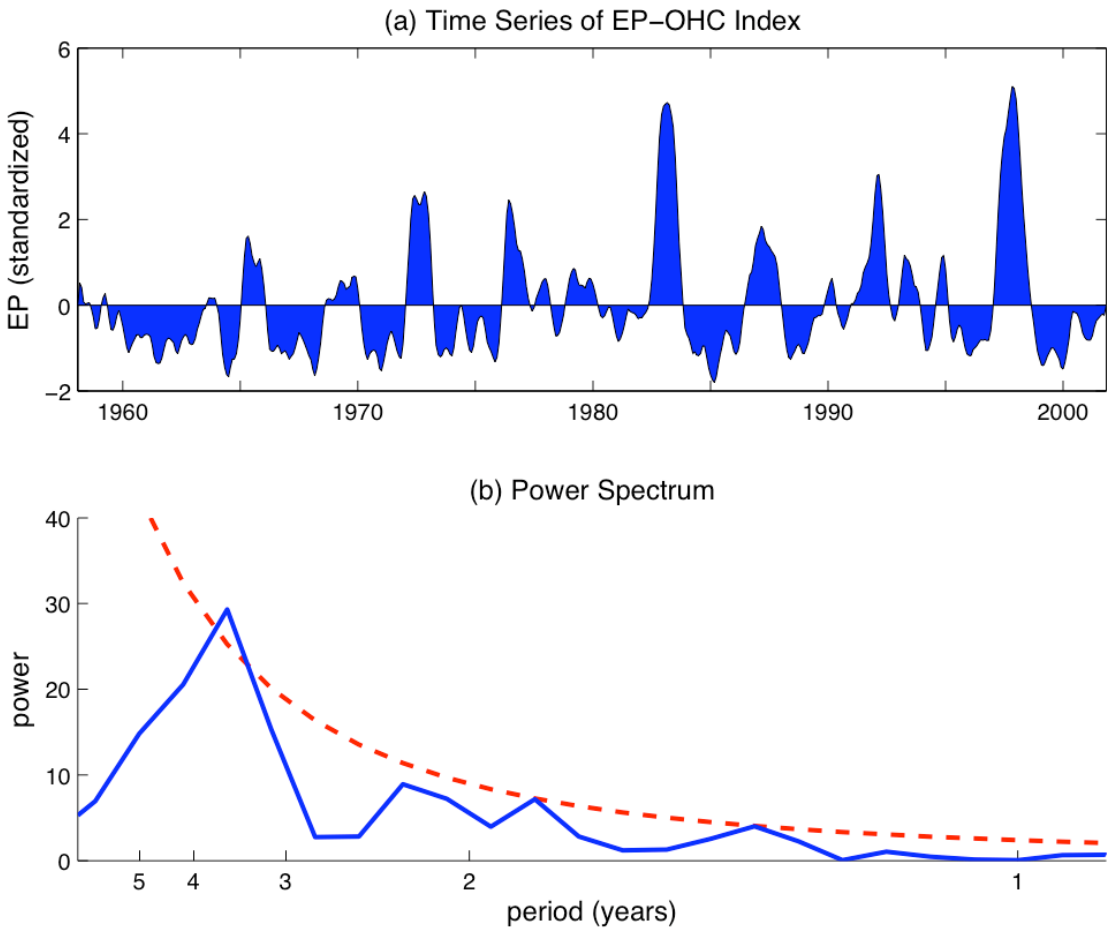


Figure 8. (a) Time series and (b) power spectrum of the normalized EP OHC index. The red curve represents the 99% significance level.

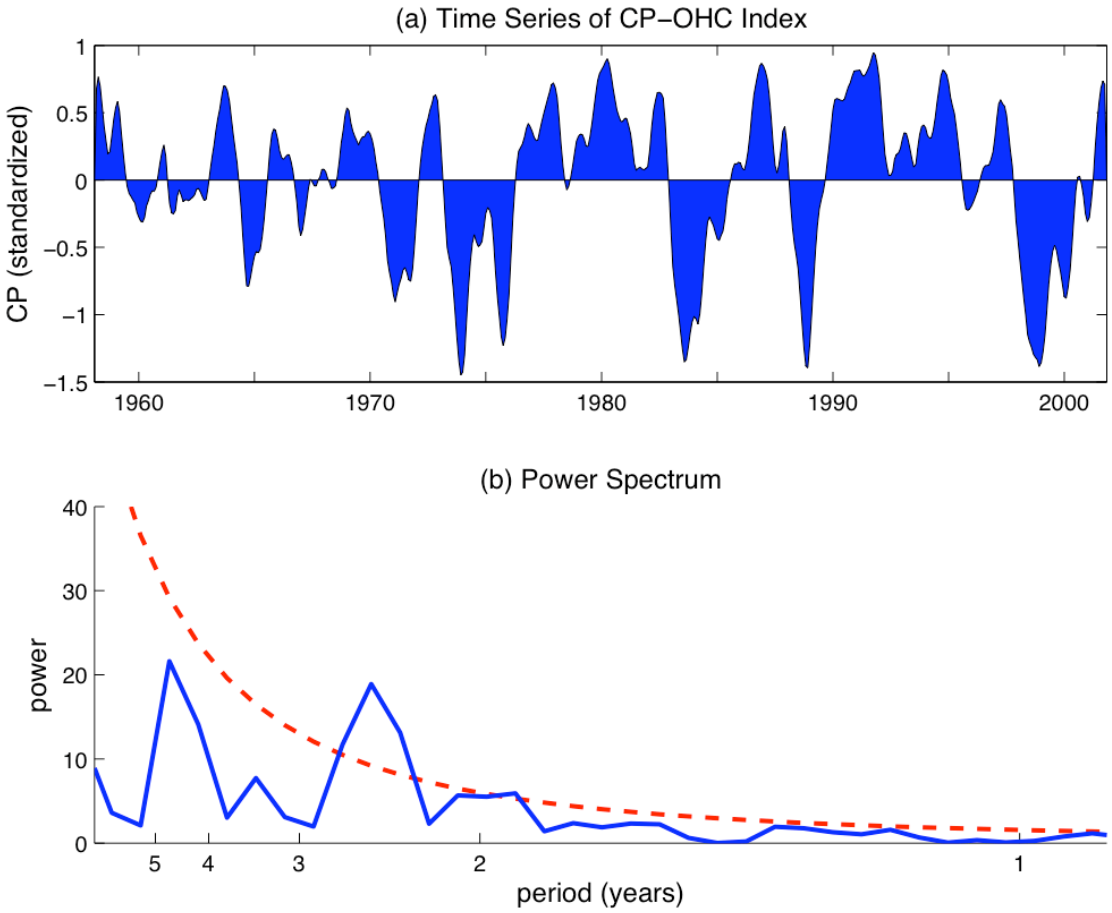
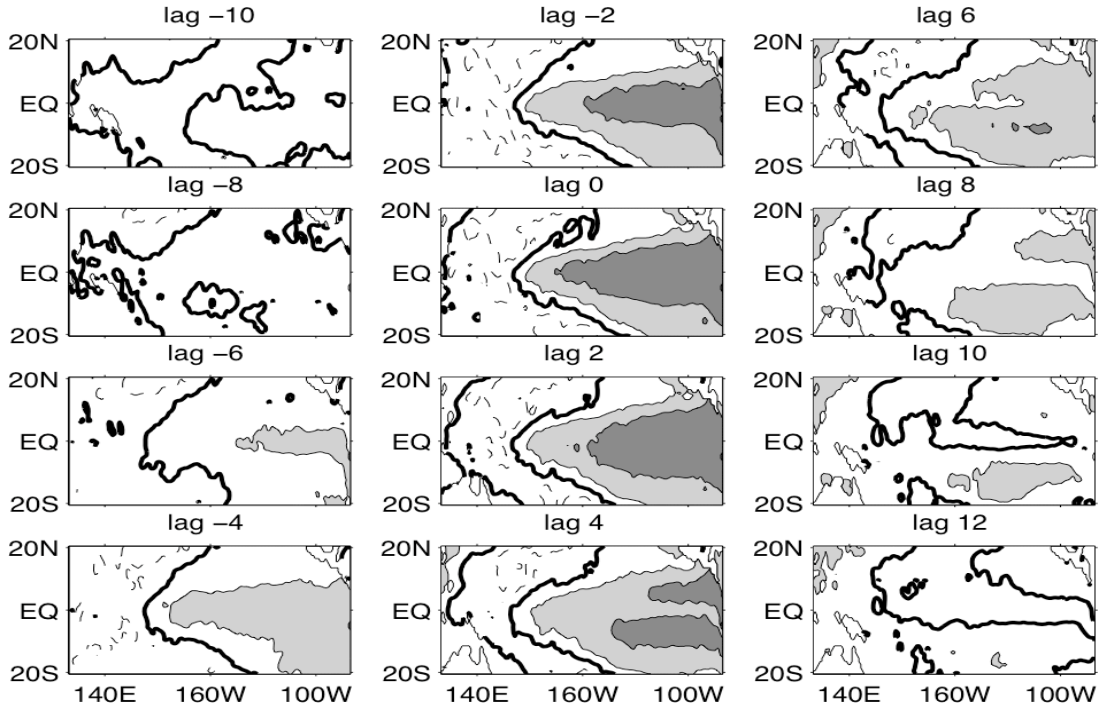


Figure 9. Same as Figure 8 but for the CP OHC index.

(a) Lagged-correlation between EP OHC index and SST



(b) Lagged-correlation between EP OHC index and ocean temperature

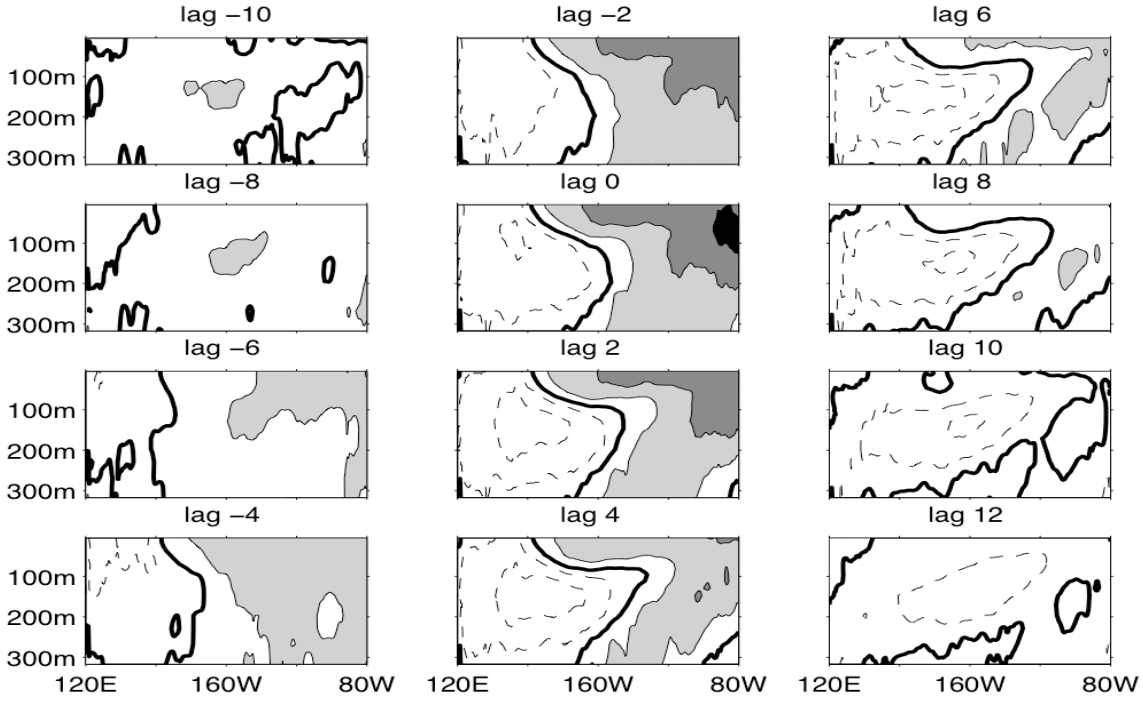
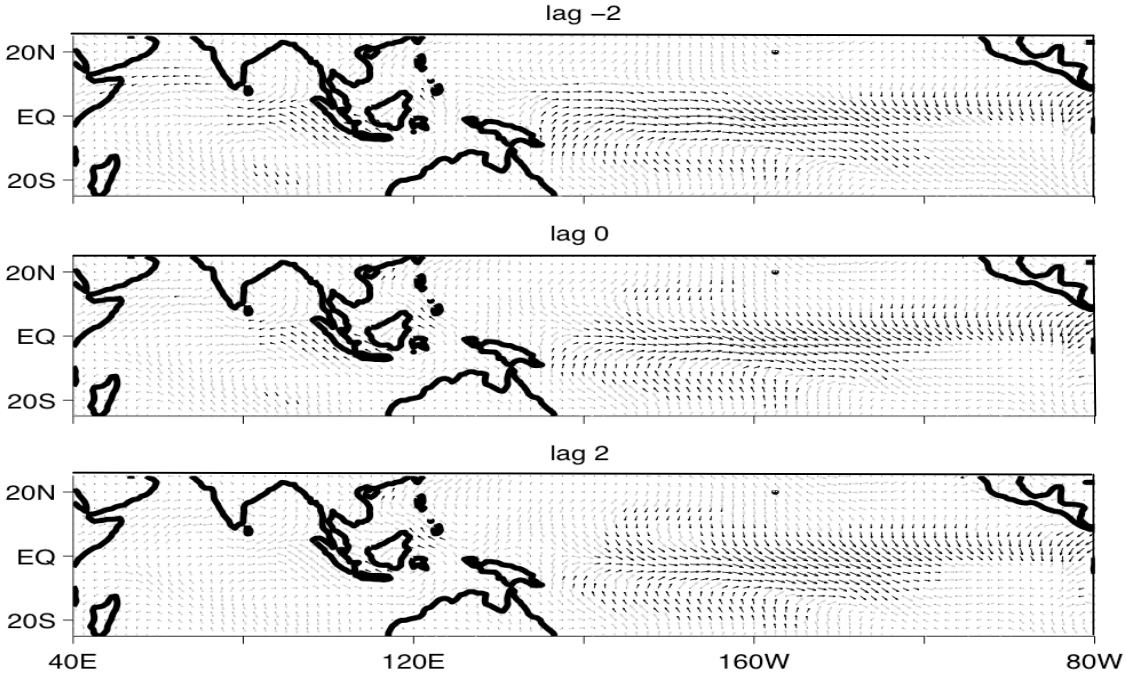


Figure 10. Lagged correlation coefficients between the EP OHC index and (a) SST anomalies and (b) subsurface ocean temperature anomalies in the tropical Pacific. Contour intervals are 0.3.

(a) Lagged-correlation between EP index and winds



(b) Lagged-correlation between CP index and winds

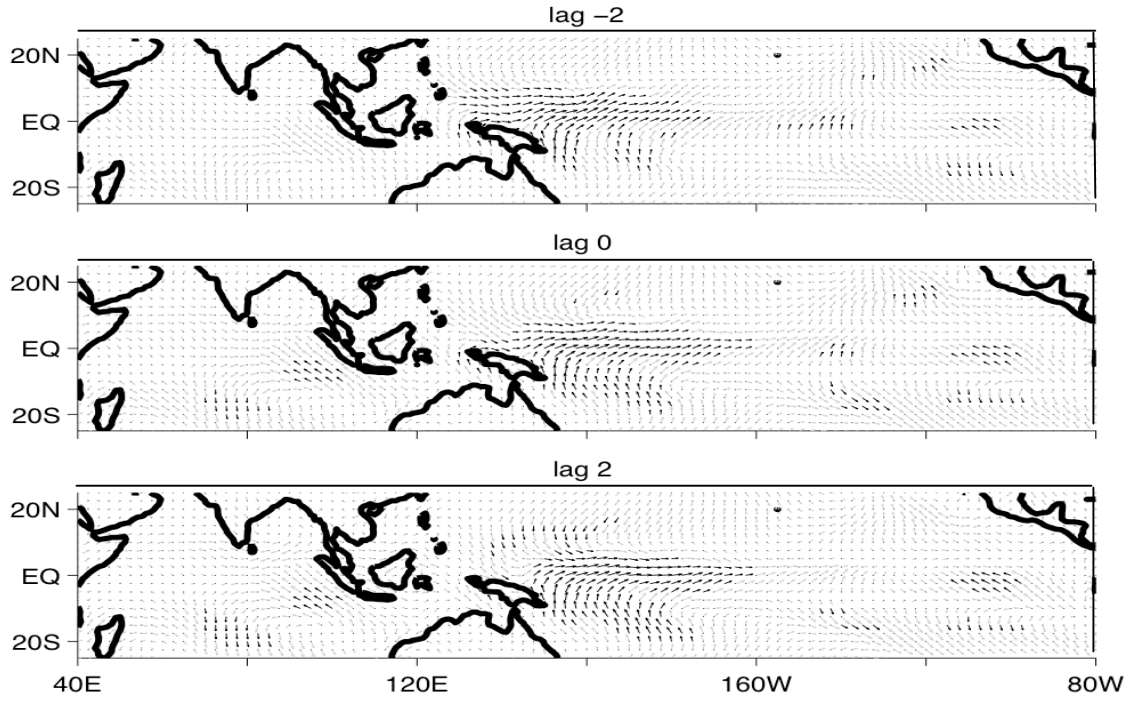
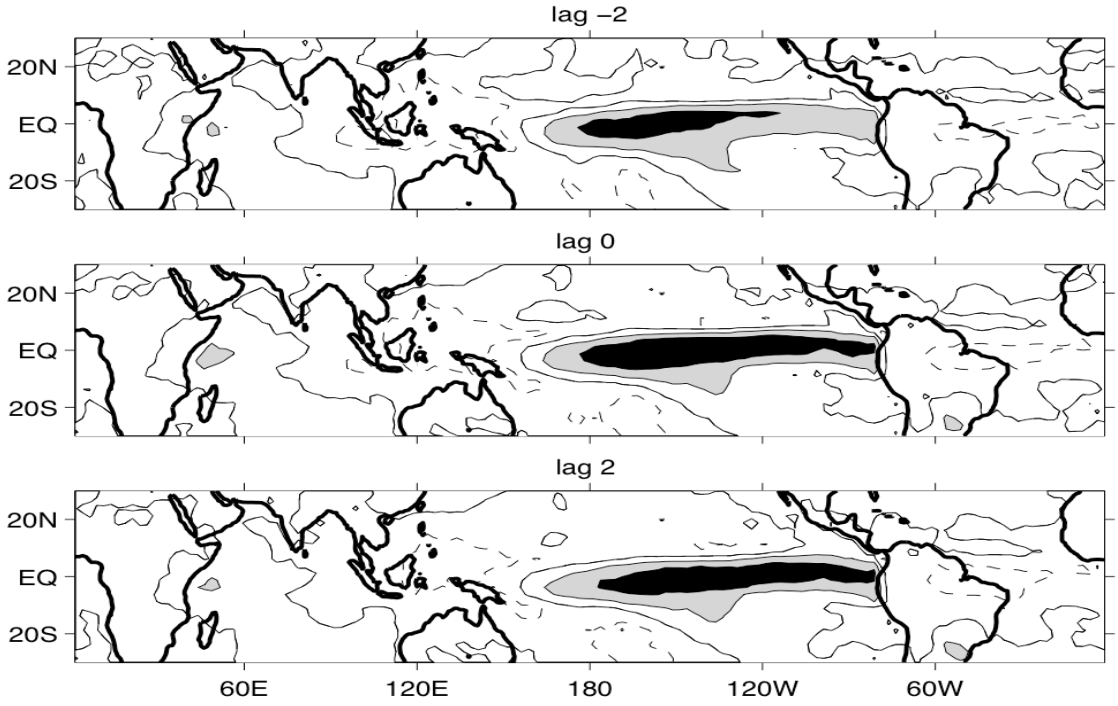


Figure 11. Lagged correlation coefficients between surface wind anomalies and the OHC index of the (a) EP-ENSO and (b) CP-ENSO. Correlation vectors that pass the 95% confidence levels are highlighted.

(a) Lagged-correlation between EP OHC index and precipitation



(b) Lagged-correlation between CP OHC index and precipitation

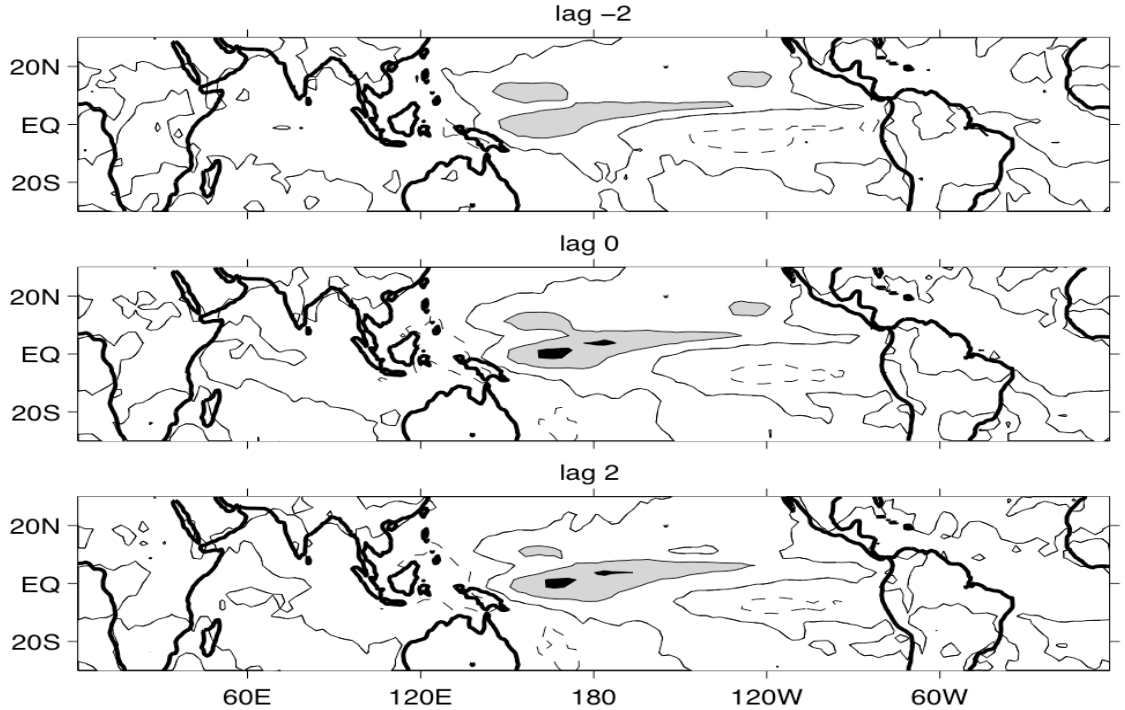
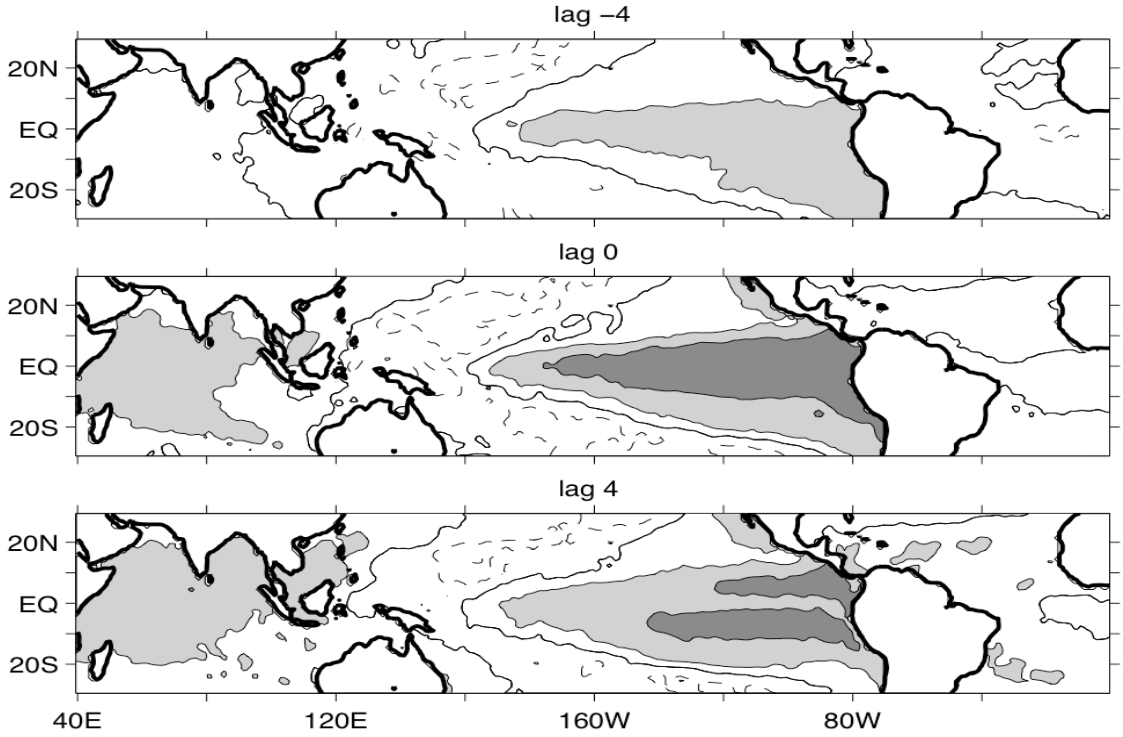


Figure 12. Lagged correlation coefficients between precipitation anomalies and the OHC index of the (a) EP-ENSO and (b) CP-ENSO. Contour intervals are 0.3 ºC.

(a) Lagged-correlation between EP OHC index and SST



(b) Lagged-correlation between CP OHC index and SST

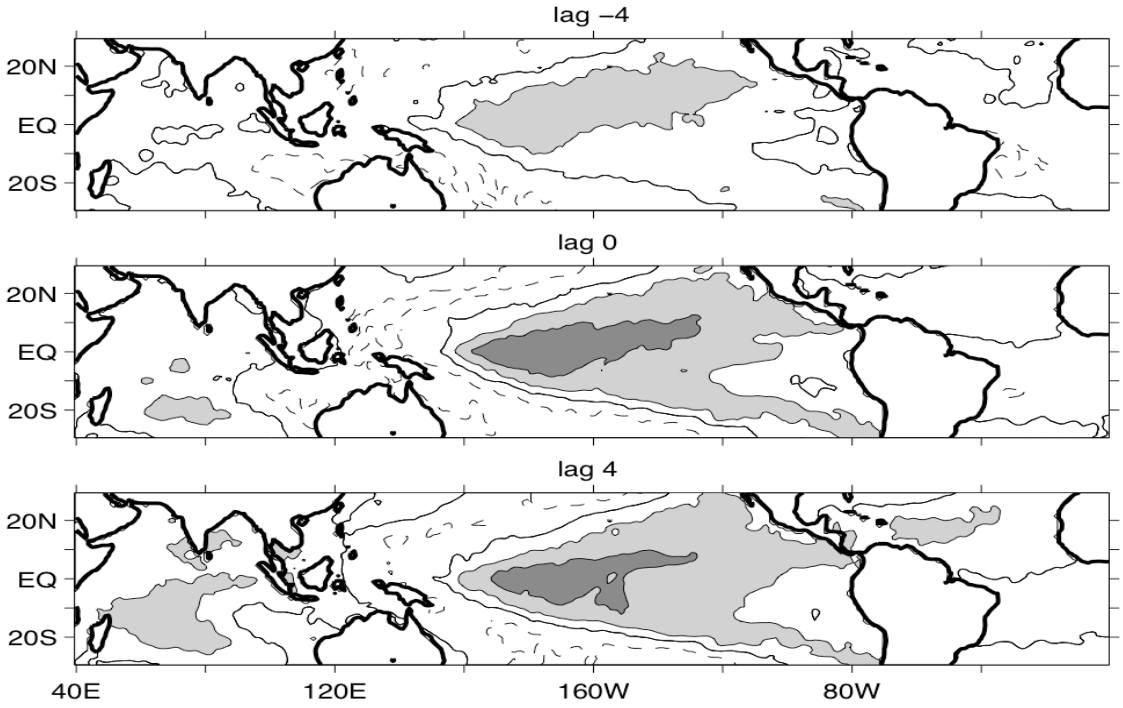


Figure 13. Lagged correlation coefficients between SST anomalies and the OHC index of (a) EP-ENSO and (b) CP-ENSO. Contour intervals are 0.3 ºC.

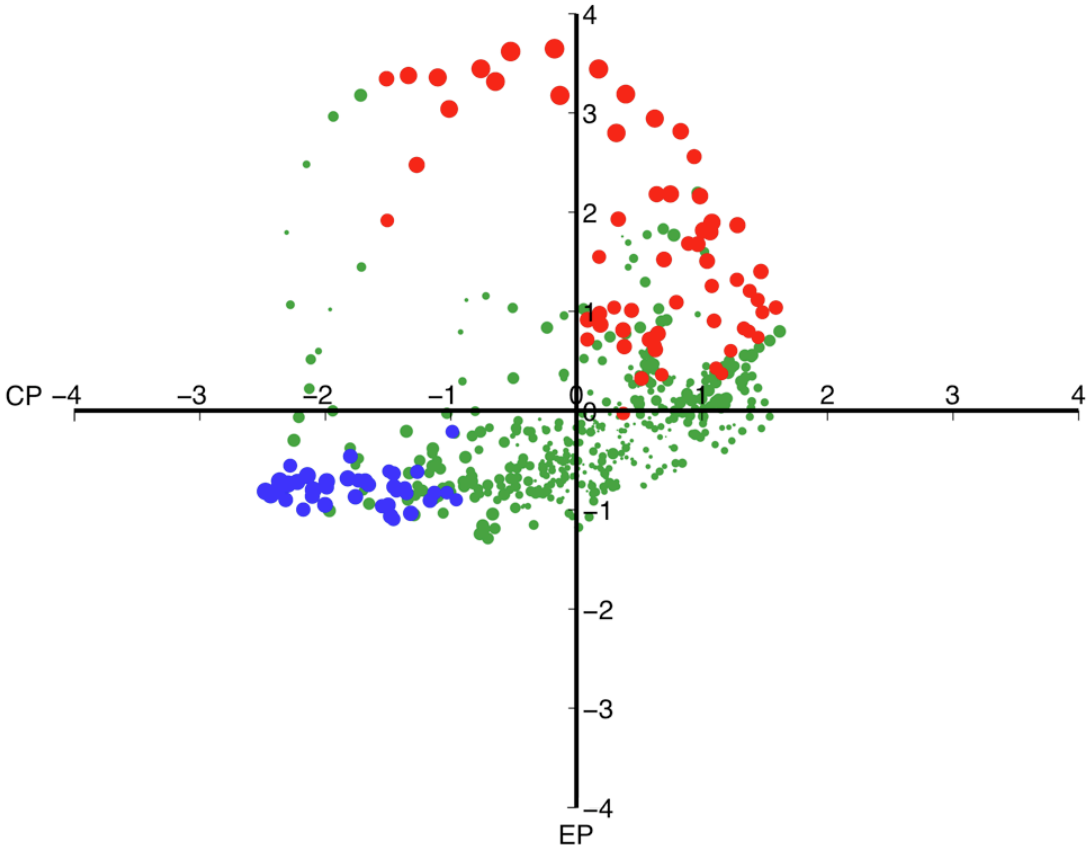
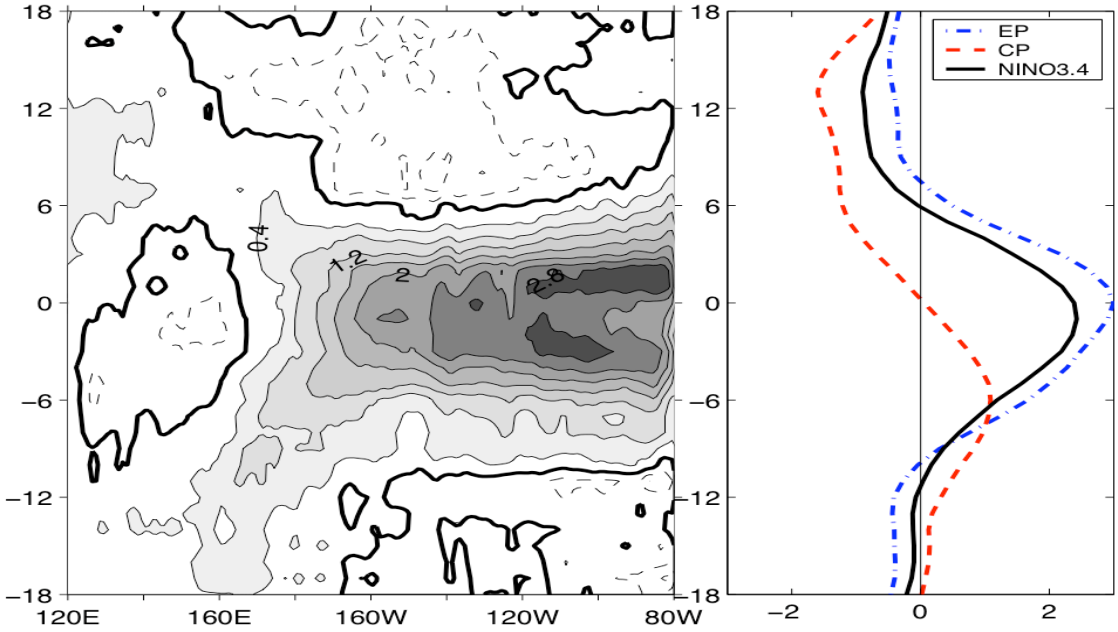


Figure 14. Scattering plot of standardized monthly values of the EP and CP OHC indices from 1958 to 2001. The dot size is proportional to the value of Niño3.4 SST index in the corresponding month. The coordinate is the value of EP OHC index. The abscissa is the value of the CP OHC index.

(a) Composite of strong EP-type of El Niño



(b) Composite of strong CP-type of La Niña

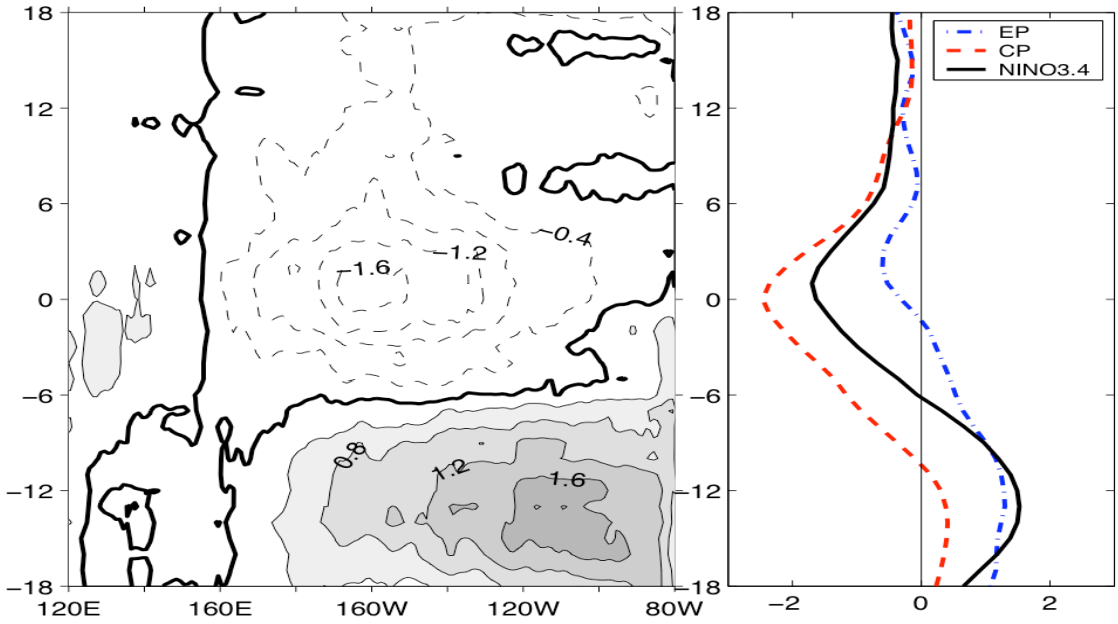


Figure 15. Composite lifecycle of SST anomalies along the eqiatorial Pacific for (a) strong EP-type of El Niño events and (b) strong CP-type of La Niña events. The center month of the composite is the month of peak value of the OHC index. Contour intervals are 0.4°C. The right panels show the corresponding EP OHC index (blue dot-dashed), CP OHC index (red dashed), and Niño3.4 SST index (black).